International Journal of Engineering Trends and Technology
ISSN: 2231–5381 / https://doi.org/10.14445/22315381/IJETT-V74I1P107

Volume 74 Issue 1, 95-107, January 2026

Original Article

Performance Evaluation of Self-Compacting Concrete Using Glass Granular Blast Furnace Slag Sand as a Partial Replacement for Manufactured Sand

Nilesh Lende[1], Smita Patil[2], Jessly Rajan[3]

[1,2,3]*Department of Civil Engineering, Datta Meghe College of Engineering, University of Mumbai, Maharashtra, India.*

[1]*Corresponding Author : nilesh.lende@dmce.ac.in*

Received: 18 July 2025 Revised: 15 December 2025 Accepted: 25 December 2025 Published: 14 January 2026

Abstract *- This paper explores the effect of Glass-Granular Blast-Furnace-Slag Sand (GGBFS sand) as a partial substitute for Manufactured Sand (M-Sand) in Self-Compacting Concrete (SCC). The purpose of the research was to determine an optimal replacement level, which would maximise performance and simultaneously lead to sustainability because of the use of industrial waste. Blends of GGBFS-sand substitutions were made in seven mixes with 0% to 60% GGBFS-sand substitutions, with a constant composition of OPC and GGBS ratio of 0.30 water-binder mix. The V-funnel, T_{50}, slump-flow, and L-box tests, alongside evaluations of mechanical performance (flexural strength, compressive, split-tensile, and modulus of elasticity) or durability (water permeability, chloride permeability, and acid resistance tests), were employed to examine the fresh properties. A digital microscopic analysis was done to read surface morphology and pore characteristics. Findings showed that 30% GGBFS-sand replacement showed the best balance in performance by giving an increment of 7% compressive strength and a decrease of 13% chloride charge passed as opposed to the control. The smoother and sub-angular texture and filler effect of slag sand were found to improve its flowability, decrease permeability, and refine surface morphology. At an above percentage of 40, excess fines formed higher viscosity and slightly reduced strength. The results affirm that GGBFS sand (when used under control) creates a stable, compact, durable concrete matrix that is self-compacting and provides efficiency in structure as well as environmental advantage. The material has high potential for sustainable construction, where workability, durability, and the saving of resources are equally important.*

Keywords *- Self-Compacting Concrete, GGBFS Sand, Manufactured Sand, Workability, Durability, Sustainable Concrete.*

1. Introduction

The extraction of river sand and the ecological imbalance created by the extraction of sand have enhanced the search to find sustainable fine aggregates for concrete. The uncontrolled mining affects the morphology of rivers, groundwater, and ecosystems [1]. Sand mining regulations on river sands have driven up the use of Manufactured Sand in India (M-sand). Even though M-sand offers uniform grading, it is produced through quarrying and mechanical crushing, which consumes a lot of power, dust, and noise emission [2, 3]. The fineness and uniformity of M-sand in high-performance mixes are reduced due to contamination by fine soil and clay in quarry sites during the monsoon. These problems make it clear that we should have an aggregate that is stable and does not require further mining and heavy processing.

The non-metallic slag sand produced during steel production (Glass-Granular Blast-Furnace-Slag Sand (GGBFS Sand) can provide such potential. It is made by the controlled air or water granulation of the melted slag, and is composed of sub-angular glassy particles of a homogeneous chemical composition with a smooth surface. Such morphology decreases internal friction and improves paste coating, which simplifies the movement of Self-Compacting Concrete (SCC) [4, 5]. GGBFS sand reuse not only avoids landfill waste but also helps the implementation of the circular-economy approach in construction [6]. It also promotes secondary hydration, which refines the matrix because of its latent hydraulic reactivity.

Studies of slag-based fine aggregates always show performance advantages at moderate replacement levels. According to Tangadagi et al. [4], the workability or compressive strength of SCC improved with steel-slag fines because it is better packed, and the micro-lubrication effect of smooth particles exists. Ahamed et al. [7] observed that a natural sand with slag fines was found to be stiffer when partially replaced. According to Rajalinggam et al. [8], the SCC with approximately 30% slag sand had better cohesiveness and reduced bleeding, and Reshma et al. [9]

correlated slag-sand concretes with reduced permeability and acid resistance. These experiments affirm that the process of slag fines-controlled addition improves the pore structure and bonding between interfaces. Blended-binder research complements findings that are discovered. Boakye and Khorami [6] demonstrated that the addition of steel slag powder with calcined clay refined pores and minimised chloride transportation by the addition of extra pozzolanic action. Nataraja et al. [10] found that structural-grade strength and long-term durability were maintained with the help of GGBS with slag sand. Kumar et al. [11] showed that SCC of high strength with the use of steel-slag fines formed dense and homogenous microstructures and reduced ionic permeability. These studies, combined, put an accent on the durability benefits of slag aggregates, but the slag sand behaviour still has not been well studied.

The use of GGBFS sand in SCC solves both the technical and environmental issues. The material removes mining, minimises transportation energy, and transforms industrial waste into a building material [12]. Its fine gradation increases packing and pore refinement, although too many fines can reduce the flow; therefore, it is necessary to know an optimal range. Although both GGBFS and GGBS have been examined independently, both GGBFS as fine aggregate and GGBS as binder are rarely researched jointly within the framework of SCC.

This dual inclusion will be complementary to the mechanism; the slag sand will act as a physical filler and enhance rheology, whereas the GGBS binder will act as a chemical additive and will form extra “Calcium Silicate Hydrate (C–S–H) or Calcium Alumino Silicate Hydrate (C–A–S–H)” during hydration [13]. A combination of these mechanisms can reduce permeability, increase chemical stability, and increase the long-term stability. Although the quantitative effect of GGBFS-sand ratio on fresh, mechanical, and durability properties is not well-defined yet, and not many researchers combine statistical and microstructural analysis to identify an optimal dosage.

The current experiment substitutes M-sand with GGBFS sand at varied amounts (0-60%) and keeps a steady cement, GGBS binder, and water-binder ratio. Slump-flow, V-funnel, or L-box tests are utilized to determine fresh properties; compressive, tensile, flexural, and modulus tests to determine mechanical behaviour; and permeability, acid-attack, and chloride-penetration tests to determine durability. The morphological and microstructural observations explain the impact of slag-sand particles on pore structure and paste-aggregate bonding. Statistical modelling determines the best replacement, which balances between workability, strength, and durability. The paper has shown that when GGBFS sand and GGBS binder are used in a coordinated manner, they create a dense, durable, and environmentally friendly SCC that could be used in sustainable construction.

2. Materials and Methods

2.1. Raw Materials

The materials have been selected based on the criteria for sustainability, availability, and performance. 53-grade Ordinary Portland Cement (OPC) or Ground-Granulated Blast-Furnace Slag (GGBS) were cementitious materials used. M-sand (Manufactured sand) or GGBFS sand served as fine aggregates, while 10mm crushed granite has been utilized as the coarse aggregate. The mix design had been completed by including potable tap water and a high-range water-reducing additive mixture from polycarboxylate-ether chemistry.

The grade of OPC 53 applied in this research had a specific gravity of 3.15 or 320m²/kg of fineness, which met the requirements of the IS 12269:1987 [14]. The supplementary binder was the GGBS with a 2.90 specific gravity or fineness of 400-450m²/kg [15]. The addition of GGBS increases the cohesiveness and segregation resistance of SCC and increases long-term strength and durability [16]. GGBFS sand, a by-product of steel production, was used as a partial substitution for M-sand. It exhibited a 2.55 specific gravity and an absorption of water of approximately 1.2%. M-sand had a particular gravity and fineness ratio of 2.67 and 2.9, respectively. The two aggregates satisfied the requirements of IS 383:2016 on the particle-size [17]. The coarse aggregate was of the specification of IS 383:2016 with a nominal maximum size of 10mm, specific gravity 2.67, and water absorption of 1.8%. The water mixing was as per the IS 456:2000 [18]. An ether form of Polycarboxylate-Ether Superplasticizer (PCE) of specific gravity 1.08 was incorporated in 0.8% of binder mass to provide successful self-compaction.

2.2. Sieve Analysis and Gradation

Particle-size distribution of the fine aggregates was determined following IS 2386 (Part 1):1963 [19]. The substitution of M-sand with GGBFS sand in 10 % increments (10–70 %) revealed a greater proportion of fines in the latter, as demonstrated in Figure 1. The fineness modulus decreased progressively from 2.84 for M-sand to 2.25 for GGBFS sand, indicating higher surface area and more intimate paste–aggregate contact. However, when replacement exceeded 50 %, excess fines increased the viscosity of the mix and compromised flowability [20].

2.3. Mix Design and Proportioning

A consistent water-to-binder ratio of 0.30 was utilized to proportion all mixes for SCC. 353 kg/m³ of OPC and 190 kg/m³ of GGBS made up the binder composition. Coarse aggregate and mixing water were kept constant at 867 kg/m³ and 160 kg/m³, respectively. M-sand was replaced with GGBFS sand in 10 % steps up to 60 %, as summarized in Table 1. Mix proportions were developed in line with IS 10262:2019 and validated against EFNARC guidelines [21, 22].

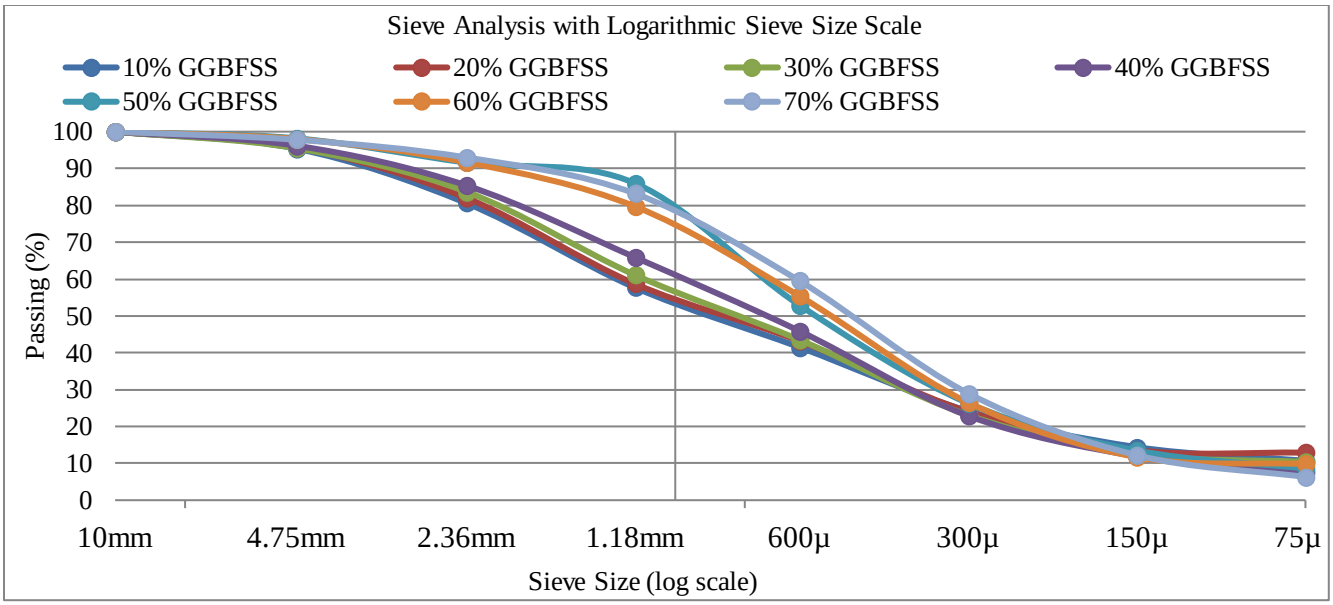

Fig. 1 Particle size distribution curves for M-Sand and GGBFS sand blends (10–70%)

2.4. Mixing Procedure and Casting

All concretes were prepared in a mechanical pan mixer following a standardized dry-wet sequence:

1. Dry blending of cement, GGBS, M-sand, and GGBFS sand to obtain a uniform powder mix.
2. Incorporation of coarse aggregate and continuation of dry mixing for 1 min.
3. Gradual addition of water and superplasticizer while maintaining continuous rotation.
4. Final mixing until a homogeneous, flowable SCC consistency was achieved.

Fresh concrete was tested immediately for flow characteristics. Specimens for strength and durability have been cast in steel moulds, demoulded after 24h, and dried in clean water at 27±2℃ for 28-56 days.

2.5. Testing and Data Analysis

Each study was performed in a regulated laboratory environment. Their fresh, mechanical, or durability properties have been evaluated. EFNARC identified the slump-flow diameter, V-funnel flow, T_{50} duration, or L-box ratio as the characteristics of fresh SCC. The properties of hardened concrete, encompassing split-tensile, flexural strength, compressive, and modulus of elasticity, were determined according to the guidelines in IS 516 [23]. Durability was measured using water-permeability, rapid-chloride-permeability (ASTM C1202-19) [24], and acid-resistance tests. The statistical processing of experimental data was carried out to determine the optimal ratio of M-sand to GGBFS sand replacement. The trends in workability, strength, and permeability were analysed to identify a balanced level of replacement, which would improve performance and sustainability.

Table 1. Trail mix design of self-compacted concrete (kg/m³)

Mix ID	OPC	GGBS	M-Sand	GGBFS Sand	10 mm Aggregate	Water	Admixture (%)
0% GGBFSS	353	190	837.0	0.0	867	160	0.80
10% GGBFSS	353	190	753.3	83.7	867	160	0.80
20% GGBFSS	353	190	669.6	167.4	867	160	0.80
30% GGBFSS	353	190	585.9	251.1	867	160	0.80
40% GGBFSS	353	190	502.2	334.8	867	160	0.80
50% GGBFSS	353	190	418.5	418.5	867	160	0.80
60 % GGBFSS	353	190	334.8	502.2	867	160	0.80

3. Results and Discussion

3.1. Fresh Properties of Self-Compacting Concrete

All SCC mixes were determined with the slump-flow test, T_{50}, V-funnel, or L-box tests (Figure 2, Table 2). These aspects define the self-levelling characteristic and the ability to flow through the reinforcement without mixing [25, 26]. The values of the slump-flow were measured to be 678mm to 712mm, which were within the EFNARC-recommended range (650-800mm). It was found that the maximum spread was at 30% at GGBFS-sand replacement (712mm), which was a significant improvement compared with the control mix (684 mm). Above 40%, the diffusion slowed down because of

the increased surface area of fine slag particles, which required additional paste to sustain a state of lubrication [9]. V-funnel test achieved a minimum flow time of 6.42s with 30% mix, which was against 7.12s with the control. The slight decrease is a sign of easier flow and less internal friction in the medium levels of substitution. V-funnel time rose to 7.8s at 60% replacement, and this indicated high viscosity due to overload of fines. The same trend was observed in T_{50} results: the lowest spread time (3.5s) was obtained at the 30% capacity, and the increased replacements delayed the initiation of the flow. Passing ability measured through the L-box (H_2/H_1) ratio also improved with slag-sand addition. Mixtures containing 20–30 % GGBFS sand recorded a ratio of 0.90, indicating unobstructed flow through simulated reinforcement. At 60 %, the ratio declined to 0.82, suggesting potential blocking. Overall, the 30 % replacement mix satisfied all EFNARC flow, viscosity, and passing-ability criteria, confirming its superior fresh performance.

Table 2. Fresh properties of SCC at different replacement levels of GGBFS sand

Trail Mix ID	Slump Flow (mm)	V-Funnel (second)	V-5 min (second)	T500 (second)	L-Box (H_2/H_1)
0-GGBFSS	684	7.12	11.5	4.23	0.87
10-GGBFSS	692	6.95	11.16	4.2	0.87
20-GGBFSS	704	6.7	10.63	3.9	0.9
30-GGBFSS	712	6.42	10.26	3.5	0.9
40-GGBFSS	706	7.13	11.23	3.6	0.88
50-GGBFSS	692	7.42	11.67	3.9	0.85
60-GGBFSS	678	7.8	11.84	4.3	0.82

(a) Slump flow test | **(b) V-Funnel test** | **(c) L-Box test"**

Fig. 2 Fresh properties test of self-compaction concrete

3.2. Compressive Strength

Compressive-strength development was monitored at 3, 7, 28, and 56 days (Figure 3). Strength increased consistently by about 30% replacement and then decreased. At 56 days, the 30% mix reached 72.5 MPa, around 7.3 % improvement over the control (67.6 MPa). The increase stems from denser packing of slag particles and pozzolanic interaction with $Ca(OH)_2$, forming additional C–S–H gel. Beyond 40 %, dilution of the binder and reduced effective paste volume caused a marginal decline in strength. Similar non-linear trends have been reported for slag-based Concrete [9, 13].

3.3. Split Tensile Strength

Tensile-strength variation mirrored the compressive-strength trend (Figure 4). A maximum of 5.5 MPa was obtained for the 30 % replacement mix (30SS-SCC), an 8 % gain over the control. This improvement reflects stronger Interfacial bonds and uniform stress transfer through a refined matrix. Replacement beyond 40 % led to marginal decreases because excessive fines introduced porosity and reduced cohesion.

3.4. Flexural Strength

Flexural strength additionally benefited from the incorporation of moderate GGBFS-sand levels (Figure 5). The 30% mix had 9.2 MPa as compared to 8.6 MPa on the control, which had less tensile resistance in bending.

There was increased microstructural continuity and uniform crack-bridging ability, which resulted in increased load-carrying capacity. Increased replacement ratios weakened the matrix, and it lost some slight performance.

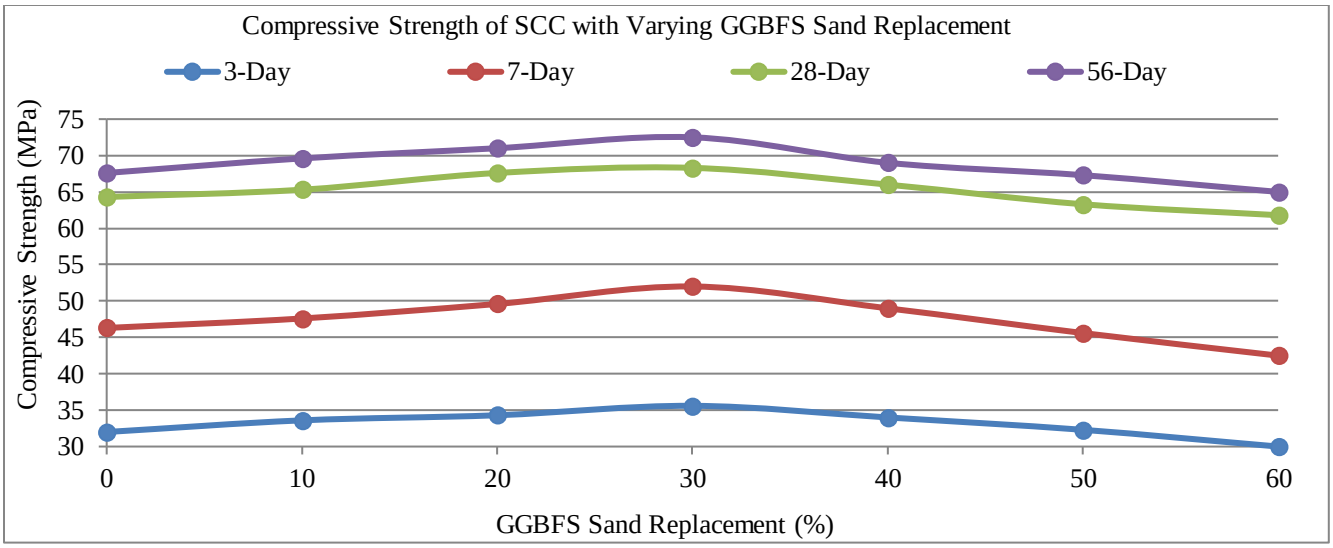

Fig. 3 Compressive strength of SCC with varying GGBFS sand replacement

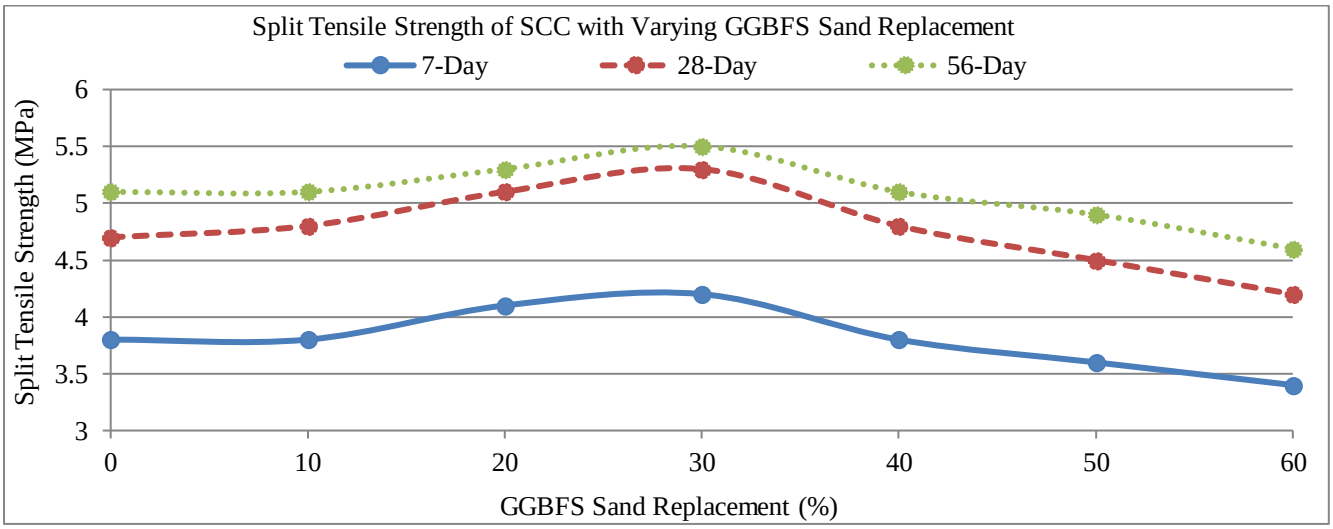

Fig. 4 Split tensile strength of SCC with varying GGBFS sand replacement

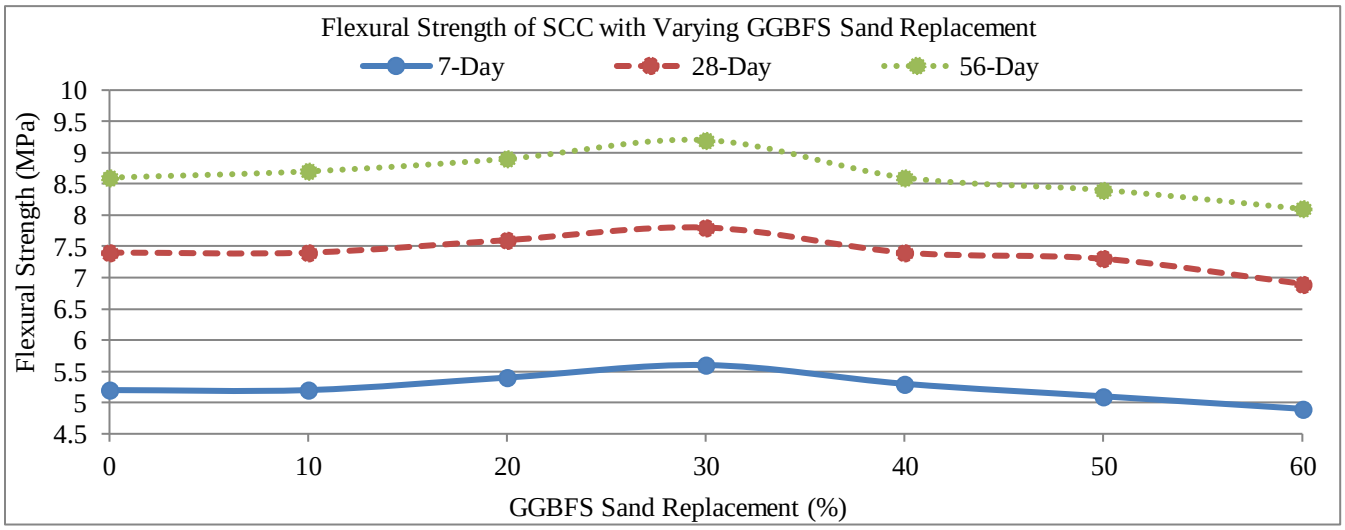

Fig. 5 Flexural strength of SCC with varying GGBFS sand replacement

3.5. Modulus of Elasticity

Incremental improvement in the elastic modulus was observed with increased GGBFS sand content to 30% which reached a pinnacle of 39.2, which illustrates an improvement in the stiffness and densification of the matrix (Refer to Figure 6). However, the introduction of excess fines, but worryingly enough, reduced the modulus beyond this point.

3.6. Resistance to Sulphuric Acid Attack

The acid resistance was also measured by the retention of compressive strength after being subjected to a sulfuric acid solution (Figure 7).

The GGBFS-sand SCC (30%) had a ratio of strength retention of 82.2%, which was greater than that of the control mix, which retained 79.9% of the initial strength. This enhancement means that GGBFS sand increased the density of the matrix and also decreased acid attack susceptibility.

The fine microstructure was effective in restricting the calcium hydroxide leaching and reduced the rate of formation of expansive degradation products, and thus enhanced stability in the long term in an acidic environment. These results are in line with reports on moderate incorporation of slag, which increases sulphate and acid resistance.

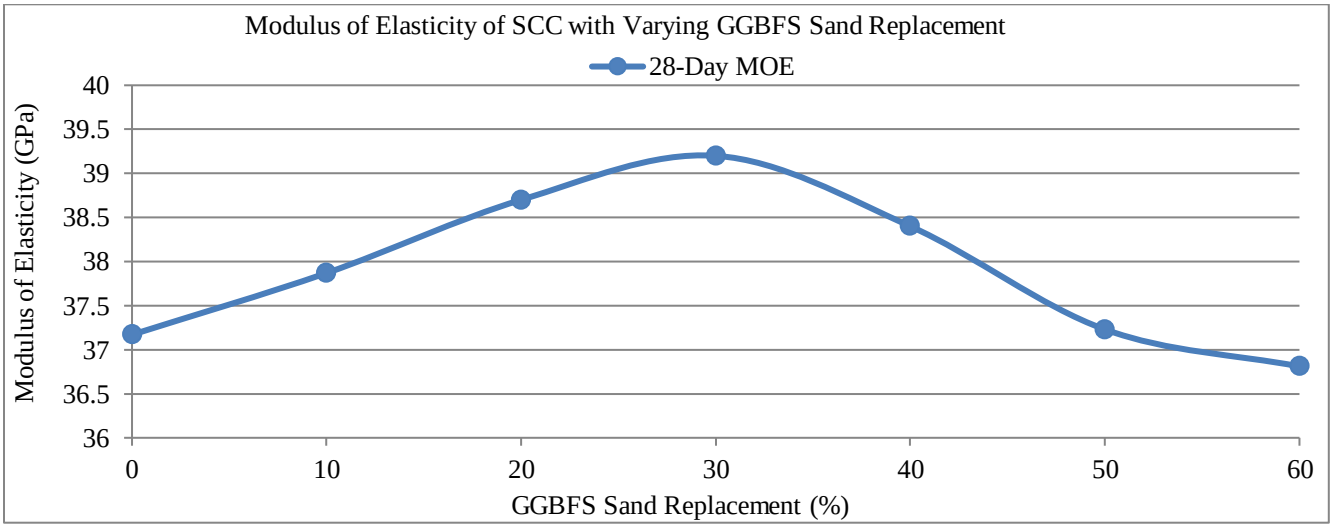

Fig. 6 Modulus of Elasticity (MOE) of SCC with varying GGBFS sand replacement

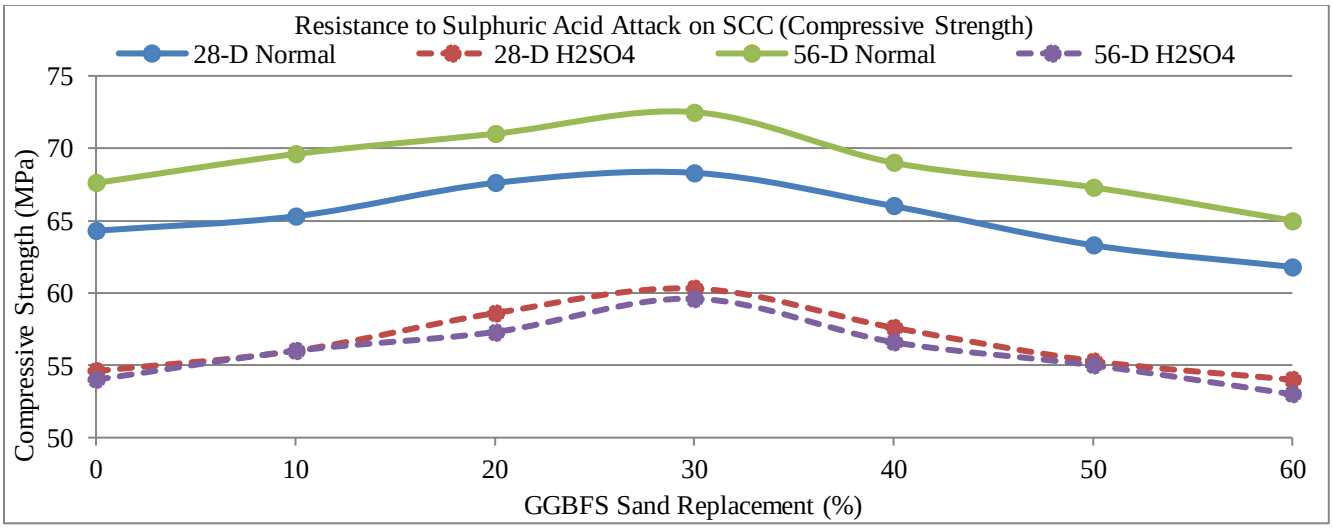

Fig. 7 Resistance to sulphuric acid attack (compressive strength of SCC)

3.7. Water Permeability

The water-permeability depth pattern was also similar, as depicted in Figure 8. Normal curing resulted in permeability reducing to 8mm at 30% replacement, which signifies refined pore connectivity. The same mixture recorded the minimum penetration (12mm) after exposure to sulphate, which confirmed that the presence of slag-sand inhibited capillary continuity during chemical attack. The slight increase at 50–60 % replacement corresponds to higher pore volume generated by surplus fines and reduced workability.

3.8. Rapid Chloride Penetration Test (RCPT)

Figure 9 presents RCPT results, showing a pronounced reduction in charge passed up to the 30 % replacement level. The charge dropped from 1780 ℃ for the control to 1540 ℃, classifying the concrete as *low-permeability* according to ASTM C1202. Sulphate-exposed specimens displayed a moderate rise in charge values (2600–2900 C) due to the formation of microcracks and secondary crystals, which partially reopened ionic pathways. Even so, the slag-modified mixes remained considerably less permeable than conventional SCC, demonstrating improved long-term resistance to chloride transport.

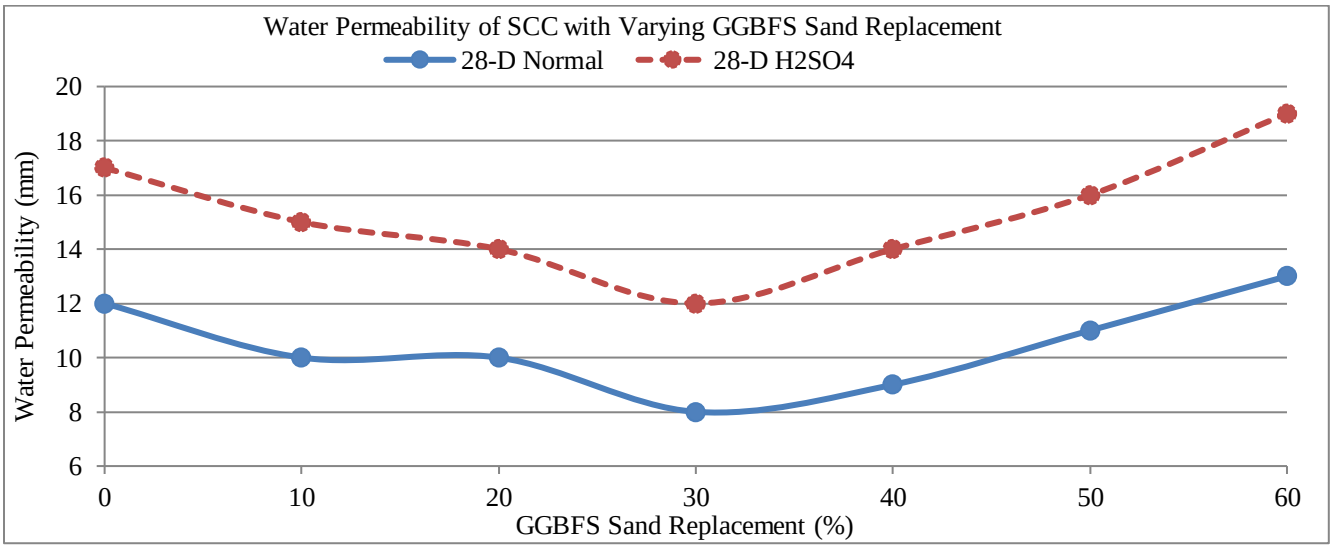

Fig. 8 Water permeability of SCC with varying GGBFS sand replacement

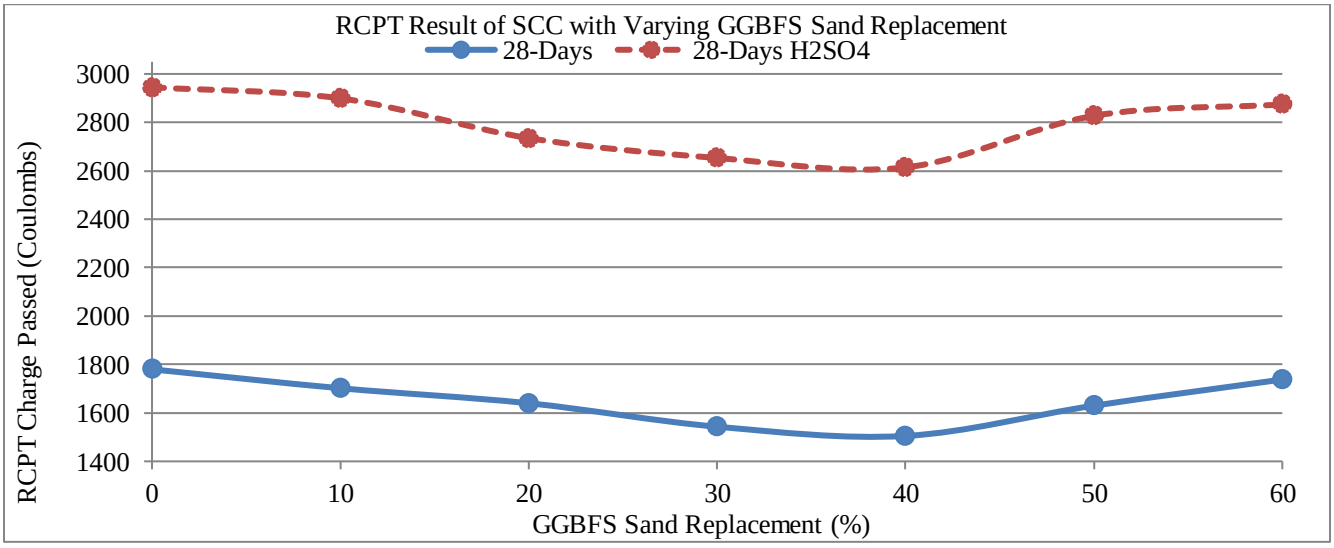

Fig. 9 RCPT result of SCC with varying GGBFS sand replacement

Table 3. Mechanical properties of SCC with varying GGBFS sand replacement

Trail Mix ID	Compression Test (MPa)				Split Tensile strength (MPa)			Flexural Strength (MPa)		MOE (GPa)
	3-D	7-D	28-D	56-D	7-D	28-D	56-D	7-D	28-D	28-D
0-GGBFSS	32	46.3	64.3	67.6	3.8	4.7	5.1	5.2	7.4	37.17
10-GGBFSS	33.6	47.6	65.3	69.6	3.8	4.8	5.1	5.2	7.4	37.87
20-GGBFSS	34.3	49.6	67.6	71	4.1	5.1	5.3	5.4	7.6	38.7
30-GGBFSS	35.6	52	68.3	72.5	4.2	5.3	5.5	5.6	7.8	39.2
40-GGBFSS	34	49	66	69	3.8	4.8	5.1	5.3	7.4	38.4
50-GGBFSS	32.3	45.6	63.3	67.3	3.6	4.5	4.9	5.1	7.3	37.23
60-GGBFSS	30	42.5	61.8	65	3.4	4.2	4.6	4.9	6.9	36.81

Table 4. Durability performance of SCC with varying GGBFS sand replacement

	Sulphur Chemical Attack (Compression test) (MPa)				Water Permeability (mm)		Rapid Chloride Penetration Test (coulomb)	
Trail Mix ID	"28-D Nomal	28-D H2SO4	56-D Nomal	56-D H2SO4	28-D Nomal	28-D" H2SO4	28 Days	28-D H2SO4
0-GGBFSS	64.3	54.6	67.6	54	12	17	1780	2945
10-GGBFSS	65.3	56	69.6	56	10	15	1702	2899
20-GGBFSS	67.6	58.6	71	57.3	10	14	1640	2735
30-GGBFSS	68.3	60.3	72.5	59.6	8	12	1543	2653
40-GGBFSS	66	57.6	69	56.6	9	14	1505	2614
50-GGBFSS	63.3	55.3	67.3	55	11	16	1630	2827
60-GGBFSS	61.8	54	65	53	13	19	1738	2874

(a) Compression Strength Specimen

(b) Split Tensile Strength Specimen

(c) Rapid Chloride Penetration Test Setup

(d) Water Penetration Test specimen

(e) Flexural Strength Test Setup

(f) Modulus of Elasticity Test Setup

Fig. 10 (a) Compression strength specimen, (b) Split tensile strength specimen, (c) Rapid chloride penetration test, (d) Water penetration test specimen, (e) Flexural strength test setup, and (f) Modulus of elasticity test setup.

4. Microscopic and Morphological Analysis

A digital microscopic study was conducted on the visual examination of the physical texture and surface morphology of SCC with GGBFS sand. Measured (a) fine-aggregate properties, (b) surface of normal and sulphate-attacked concrete, and (c) NaOH side of specimens after the Rapid-Chloride-Permeability Test (RCPT). This has been done to associate surface attributes with the experimental strengths, flow, and durability observations.

4.1. Fine-Aggregate Morphology

Digital micrographs of M-sand and GGBFS-sand particles are provided in Figure 11. The m-sand particles can be seen to be angular, dark in colour, and sharp-edged, which means that they have a mechanically crushed texture. This irregularity adds internal friction in the mixing process and necessitates an increase in paste for lubrication. Conversely, GGBFS-sand particles have glassy and smoother sub-angular surfaces that are of a lighter colour and rounded corners. This morphology will increase the packing density and allow even coating of the paste to minimise voids, and give the paste better flowability. The visual contrast is used to explain the increased slump-flow and lower V-funnel time at moderate GGBFS-sand contents.

4.2. Normal vs Sulphate-Attacked Surface Morphology

Figure 12 illustrates the surface of the normal and sulphate-attacked 30% GGBFS-sand SCC specimens. The normal specimen was thick and compact with a well-bonded granular texture and had no visible porosity. Aggregate boundaries were smooth and continuous upon reflection of sufficient self-compaction and homogenous hydration. The specimen covered by sulphate showed light surface roughness and pale deposits along fine microcracks; however, due to a limited formation of gypsum or ettringite. These slight modifications notwithstanding, the general structure of the matrix was coherent and not much disturbed, which proved the high resistance of the mix to the acid-sulphate reaction. The denser, crack-free morphology of the normal specimen and the controlled deterioration of the sulphate-exposed surface correspond closely with the strength-retention (82 %) and reduced permeability results discussed in Sections 3.6 and 3.7.

4.3. NaOH-Side RCPT Surface Morphology

Figure 13 shows the NaOH-side surfaces of GGBFS-sand SCC specimens examined after completion of the RCPT. The normal 30 % GGBFS-sand SCC specimen exhibited a tightly packed surface with uniform granular texture and very few visible pores. The dense arrangement of hydration products indicates limited ionic transport through the matrix. During the six-hour RCPT exposure, which corresponds to the low charge-passed value of about 1540 C reported in Section 3.8. In contrast, the sulphate-attacked RCPT specimen displayed slightly roughened regions, narrow surface cracks, and the presence of small crystalline deposits along micro-voids. These surface irregularities are associated with minor expansion and micro-etching produced by the sulphate reaction. The formation of such discontinuities increased the pore connectivity, allowing easier ionic movement; consequently, the total charge passed for the sulphate-exposed specimen was higher than that of the normal sample.

Overall, the visual evidence confirms that sulphate exposure compromises the otherwise dense microstructure of GGBFS-sand SCC.

However, the extent of deterioration remains considerably lower than that observed in mixes without slag-sand modification.

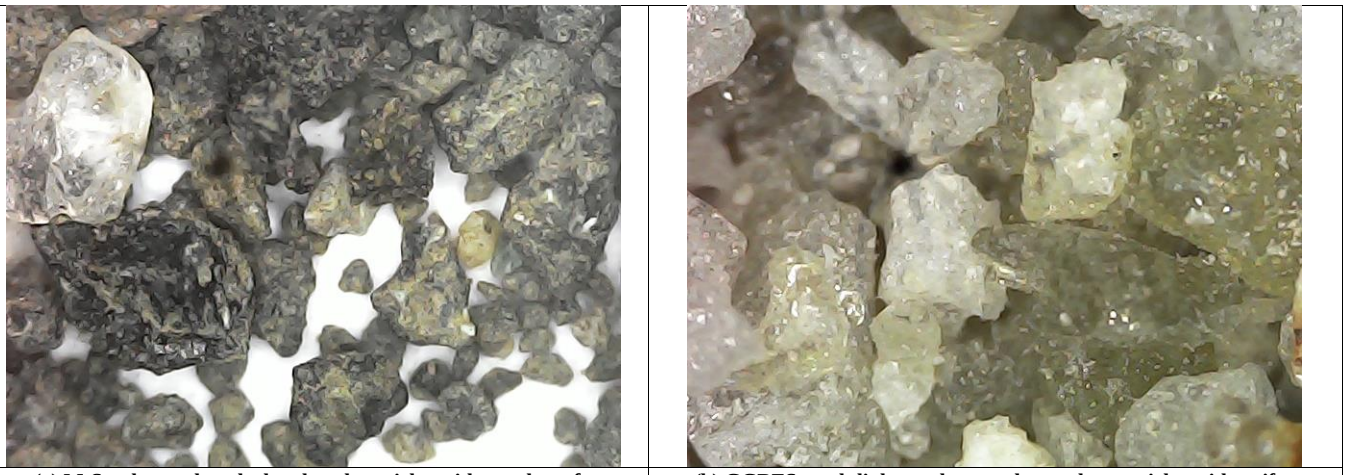

(a) M-Sand: angular, dark-colored particles with rough surface texture	(b) GGBFS sand: lighter, glassy, sub-angular particles with uniform morphology

Fig. 11 Digital microscope images showing fine-aggregate morphology, (a) M-Sand, and (b) GGBFS-sand.

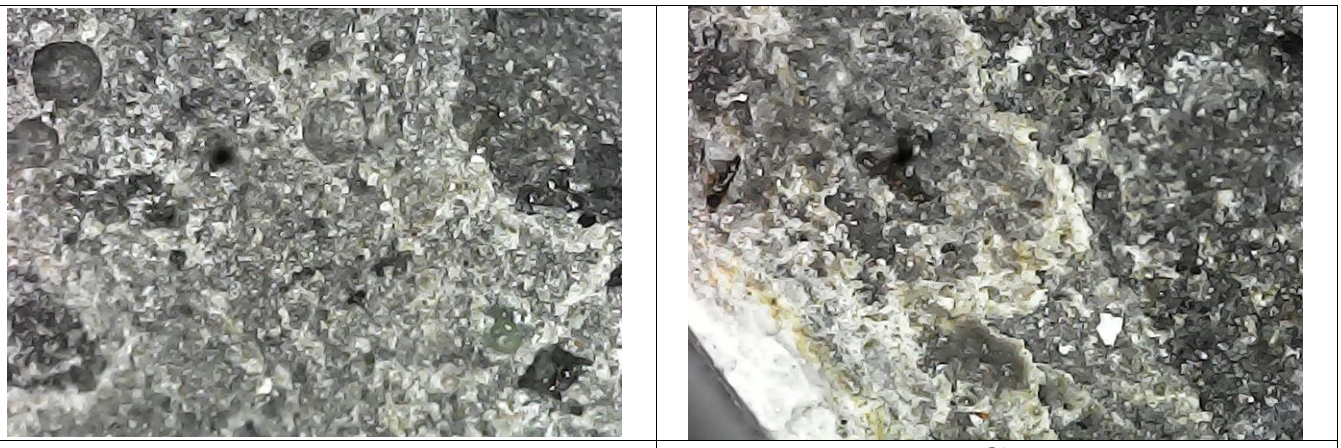

(a)	(b)

Fig. 12 Digital micrographs of GGBFS-Sand SCC surfaces, (a) Normal condition, and (b) Sulphate-attacked condition.

(a) Normal concrete surface	(b) Sulphate-attacked condition

Fig. 13 NaOH-side surfaces of GGBFS-sand SCC after RCPT testing, (a) Normal specimen, and (b) Sulphate-attacked specimen.

5. Statistical Correlation and Regression Analysis

Figure 14 illustrates the combined normalized polynomial trendlines for the various fresh, mechanical, and durability properties of SCC at different GGBFS replacement levels. At the same time, Table 5 presents the corresponding second-order regression equations and R^2 values. A second-order polynomial regression model was used to quantify the relationship between GGBFS replacement (%) and each performance parameter, expressed in the form $Y=aX^2+bX+C$. The model effectively captures the characteristic rise–peak–decline pattern observed across workability and strength properties, as well as the decline–minimum–increase trend noted in permeability-related parameters. The regression constants were obtained using least-squares fitting, and the goodness of fit was validated using the coefficient of determination (R^2), which ranged from 0.85 to 0.95, indicating strong agreement between predicted and observed results. Figure 14 and Table 5 trends indicate a consistent optimum response at approximately 25% to 35% GGBFS replacement, at which the flowability and passing ability are optimum, compressive strength and tensile strength are optimum, and flexural strength is optimum. At the same time, indicators of durability like water penetration and RCPT charge passed show their lowest values at or near the same replacement level, which implies the loss of connectivity between the pores and the increased resistance to chloride ingress. These statistical results support the experimental ones and prove that the moderate inclusion of GGBFS will result in a more conclusive and solid SCC structure. Additionally, the regression equations can be utilised as a convenient predictive model to estimate the performance of SCC without having to conduct repeated lab experiments.

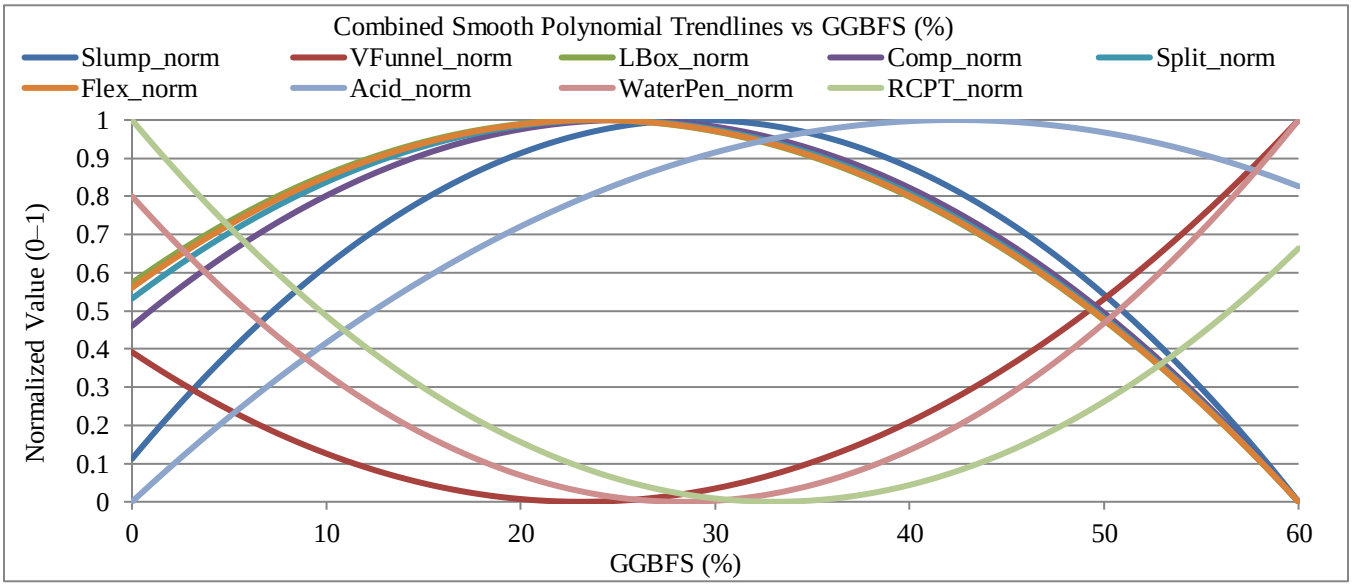

Fig. 14 Normalized polynomial trendlines showing the effect of GGBFS replacement on SCC properties

Table 5. Polynomial equations and R^2 values for SCC properties at different GGBFS replacement levels

Property	Polynomial Equation ($y = ax^2 + bx + c$)	R^2	Optimum GGBFS%	Peak / Min Value	Interpretation
Slump (mm)	y = -0.031905x² + 1.857143x + 681.190476	0.9417	29.10%	708.22 mm	Max flowability
V-Funnel (s)	y = 0.000885x² - 0.040893x + 7.154048	0.8685	23.12%	6.68 s (minimum)	Best flow time
L-Box Ratio	y = -0.000058x² + 0.002750x + 0.863333	0.9236	23.57%	0.896	Best passing ability
Compressive Strength (56d, MPa)	y = -0.005595x² + 0.284286x + 67.602381	0.9032	25.40%	71.21 MPa	Peak strength
Split Tensile Strength (28d, MPa)	y = -0.000762x² + 0.037143x + 4.647619	0.8729	24.38%	5.10 MPa	Peak tensile resistance
Flexural Strength (28d, MPa)	y = -0.000560x² + 0.026786x + 7.323810	0.8520	23.94%	7.64 MPa	Peak flexural capacity

Acid Resistance Retention (%)	$y = -0.001618x^2 + 0.137036x + 84.800714$	0.8604	42.35%	87.70%	Best acid durability at higher GGBFS
Water Penetration (mm) ***(lower = better)***	$y = 0.004286x^2 - 0.242857x + 12.142857$	0.9032	28.33%	8.70 mm (minimum)	Lowest permeability
RCPT (Coulombs) ***(lower = better)***	$y = 0.236071x^2 - 15.610714x + 1809.714286$	0.8735	33.06%	1551.64 Coulombs (minimum)	Best chloride resistance

6. Conclusion

In this study, the researcher investigated the possibility of using Glass-Granular Blast-Furnace-Slag "sand (GGBFS sand) as a sustainable partial substitute for M-sand in SCC. It has been determined in the study that the incorporation of GGBFS sand in a controlled manner is an effective way of enhancing fresh or hardened properties of SCC, and also minimizes the environmental effects of SCC.

Flowability and filling capacity rose to approximately 30% replacement, which was due to the less coarse surface and smaller particle gradation of slag sand. Above this point, surplus fines would increase viscosity and limit diffusion. The maximum proportion of the same resulted in the maximum mechanical strength, and tensile and flexural performance improved to about 72 MPa in 56 days. Durability tests revealed that the chloride permeability and the water penetration decreased significantly, which affirmed the optimization of the pore network. The strength-retention ratio was improved to 82% after acid exposure, and this is a positive indication of chemical stability. These advantages were graphically demonstrated by the digital images in the microscopes, with slag-sand SCC having a compact and uniform matrix and few microcracks as opposed to the control. The findings prove that the role of the physical densification with fillers and not the chemical reaction is decisive in enhancing performance.

Additionally, the substitution of a part of mined sand by an industrial by-product encourages the activities of the circular economy and eliminates the ecological burden of aggregate mining. In summary, the 30 % GGBFS-sand replacement level provided the most balanced combination of flowability, strength, and durability. The material presents a technically viable and environmentally responsible alternative for future SCC development, bridging sustainability with high-performance construction practice.

Acknowledgments

The authors wish to express gratitude to the "Civil Engineering Department of Datta Meghe College of Engineering, Navi Mumbai," for providing the necessary facilities and support. The authors also gratefully acknowledge JSW Cement and SIKA for their material support and contributions during the experimental phase of this study.

References

[1] Saurabh Singh et al., "Finding Alternative to River Sand in Building Construction," *Evergreen*, vol. 9, no. 4, pp. 973-992, 2022. [CrossRef] [Google Scholar] [Publisher Link]

[2] Vijaya Bhoopathy, and Senthil Selvan Subramanian, "The Way Forward to Sustain Environmental Quality through Sustainable Sand Mining and the use of Manufactured Sand as an Alternative to Natural Sand," *Environmental Science and Pollution Research*, vol. 29, no. 21, pp. 30793-30801, 2022. [CrossRef] [Google Scholar] [Publisher Link]

[3] Shivang Jayswal, and Mahesh Mungule, "Assessment of M-Sand as Potential Substitute for Natural Sand in Concrete" *International Conference on Advances in Construction Materials and Structures (ACMS-2018), IIT Roorkee*, Roorkee, Uttarakhand, India, vol. 2019, pp. 7-8, 2018. [Google Scholar]

[4] Ranjitha B Tangadagi et al., "Utilization of Steel Slag as an Eco-Friendly Material in Concrete for Construction," *Journal of Green Engineering*, vol. 10, no. 5, pp. 2408-2419, 2020. [Google Scholar]

[5] S. Praveen Nayak, "Self - Compacting Concrete using Slag Sand as Fine Aggregate," *International Journal of Science and Research (IJSR)*, vol. 12, no. 3, pp. 411-414, 2023. [CrossRef] [Publisher Link]

[6] Kwabena Boakye, and Morteza Khorami, "Properties of Self-Compacting Concrete (SCC) Prepared with Binary and Ternary Blended Calcined Clay and Steel Slag," *Infrastructures*, vol. 9, no. 3, pp. 1-16, 2024. [CrossRef] [Google Scholar] [Publisher Link]

[7] Sayed Sabbir Ahamed, and Ar. Nasreen Parvez, "Slag Sand as a Sustainable Fine Aggregate: Comparative Performance and Impacts in Concrete Relative to Natural River Sand," *Journal of Advance and Future Research (JAAFR)*, vol. 3, no. 10, pp. 202-207, 2025. [Google Scholar] [Publisher Link]

[8] Dharmaraj Rajalinggam et al., "Durability Characteristics on Self-Compacting Concrete using Casting Slag as Fine Aggregate," *Matter (Rio de Janeiro)*, vol. 30, pp. 1-6, 2025. [CrossRef] [Google Scholar] [Publisher Link]

[9] T.V. Reshma et al., "Evaluation of Strength, Durability, and Microstructure Characteristics of Slag-Sand-Induced Concrete," *Cleaner Materials*, vol. 10, pp. 1-16, 2023. [CrossRef] [Google Scholar] [Publisher Link]

[10] M.C. Nataraja et al., "Effective Utilization of Slag Sand and Ground Granulated Blastfurnace Slag for the Production of Green and Sustainable Concrete," *Indian Journal of Advances in Chemical Science*, pp. 201-205, 2016. [Google Scholar] [Publisher Link]

[11] B. Narendra Kumar, A. Meghanadh Reddy, and P. Sai Vineela, "Development of Sustainable high Performance Self Compacting Concrete using Construction and Demolition Waste and Steel Slag," *Discover Civil Engineering*, vol. 2, no. 1, pp. 1-22, 2025. [CrossRef] [Google Scholar] [Publisher Link]

[12] Zhengyi Ren, and Dongsheng Li, "Application of Steel Slag as an Aggregate in Concrete Production: A Review," *Materials*, vol. 16, no. 17, pp. 1-23, 2023. [CrossRef] [Google Scholar] [Publisher Link]

[13] Suiwei Pan et al., "Experimental Study on the Workability and Stability of Steel Slag Self-Compacting Concrete," *Applied Sciences*, vol. 10, no. 4, pp. 1-15, 2020. [CrossRef] [Google Scholar] [Publisher Link]

[14] IS 12269:1987 - Specification for 53 Grade Ordinary Portland Cement, Bureau of Indian Standards, New Delhi, 1987. [Online]. Available: https://law.resource.org/pub/in/bis/S03/is.12269.1987.pdf

[15] IS 16714:2018 - Ground Granulated Blast Furnace Slag for use in Cement, Mortar and Concrete - Specification, Bureau of Indian Standards, New Delhi, 2018. [Online]. Available: https://standardsbis.bsbedge.com/BIS_SearchStandard.aspx?Standard_Number=IS%2016714&id=23059

[16] Chiranjeevi Tadi, and T. Chandrasekhar Rao, "Investigating the Performance of Self-Compacting Concrete Pavement Containing GGBS," *Materialstoday: Proceedings*, vol. 49, pp. 2013-2018, 2022. [CrossRef] [Google Scholar] [Publisher Link]

[17] IS 383: 1970 - Specification for Coarse and Fine Aggregates from Natural Sources for Concrete, Bureau of Indian Standards, New Delhi, 2016. [Online]. Available: https://law.resource.org/pub/in/bis/S03/is.383.1970.pdf

[18] IS 456: 2000 - Plain and Reinforced Concrete - Code of Practice, Bureau of Indian Standards, New Delhi, 2000. [Online]. Available: https://law.resource.org/pub/in/bis/S03/is.456.2000.pdf

[19] IS 2386-4:1963 - Methods of Test for Aggregates for Concrete, Part 4: Mechanical Properties, Bureau of Indian Standards, New Delhi, 2002. [Online]. Available: https://law.resource.org/pub/in/bis/S03/is.2386.4.1963.pdf

[20] M. Harini, G. Shaalini, and G. Dhinakaran, "Effect of Size and Type of Fine Aggregates on Flowability of Mortar," *KSCE Journal of Civil Engineering*, vol. 16, no. 1, pp. 163-168, 2012. [CrossRef] [Google Scholar] [Publisher Link]

[21] IS 10262: 2019 - Guidelines for Concrete Mix Design Proportioning, Bureau of Indian Standards, New Delhi, 2019. [Online]. Available: https://law.resource.org/pub/in/bis/S03/is.10262.2009.pdf

[22] EFNARC, Specification and Guidelines for Self-Compacting Concrete, European Federation of National Associations Representing for Concrete, 2005. [Online]. Available: https://efnarc.org/publications

[23] IS 516: Part 1: Sec 1: 2021: Hardened Concrete Methods of Test part 1 Testing of Strength of Hardened Concrete Section 1 Compressive, Flexucal and Split Tensile Strength (First Revision), Bureau of Indian Standards, New Delhi, 2021. [Online]. Available: https://standardsbis.bsbedge.com/BIS_SearchStandard.aspx?Standard_Number=IS%20516%20:%20Part%201%20:%20Sec%201&id=34006

[24] "*ASTM C1202-19: Standard Test Method for Electrical Indication of Concrete's Ability to Resist Chloride Ion Penetration*," ASTM International, 2019. [CrossRef] [Publisher Link]

[25] IS 1199: Part 6: 2018: Fresh Concrete - Methods of Sampling, Testing and Analysis Part 6 Tests on Fresh Self Compacting Concrete (First Revision), Bureau of Indian Standards, New Delhi, 2018. [Online]. Available: https://standardsbis.bsbedge.com/BIS_SearchStandard.aspx?Standard_Number=IS%201199%20:%20Part%206&id=23797

[26] Hajime Okamura, and Masahiro Ouchi, "Self-Compacting Concrete," *Journal of Advanced Concrete Technology*, vol. 1, no. 1, pp. 5-15, 2003. [CrossRef] [Google Scholar] [Publisher Link]